1 **Manuscript**

2 *Prdm16* mutation determines sex-specific cardiac metabolism and identifies two
3 novel cardiac metabolic regulators

4 Jirko Kühnisch[1,2,3], Simon Theisen[1,2,3], Josephine Dartsch[1,2], Raphaela Fritsche-Guenther[4],
5 Marieluise Kirchner[5,6], Benedikt Obermayer[7], Anna Bauer[4], Anne-Karin Kahlert[8,9,10], Michael
6 Rothe[11], Dieter Beule[2,7], Arnd Heuser[2], Philipp Mertins[5,6], Jennifer A. Kirwan[4], Nikolaus
7 Berndt[12], Calum A. MacRae[13], Norbert Hubner[2,3], Sabine Klaassen[1,2,3,14]

8

9 *1 Experimental and Clinical Research Center, a cooperation between the Max Delbrück Center for*
10 *Molecular Medicine in the Helmholtz Association and Charité - Universitätsmedizin Berlin, Germany;*

11 *2 Max Delbrück Center for Molecular Medicine in the Helmholtz Association (MDC), Berlin, Germany;*

12 *3 DZHK (German Centre for Cardiovascular Research), partner site Berlin, Berlin, Germany;*

13 *4 Berlin Institute of Health (BIH) at Charité - Universitätsmedizin Berlin, BIH Metabolomics Platform,*
14 *Berlin, Germany;*

15 *5 Max-Delbrück-Center for Molecular Medicine in the Helmholtz Association (MDC), Proteomics*
16 *Platform, Berlin, Germany;*

17 *6 Berlin Institute of Health (BIH) at Charité - Universitätsmedizin Berlin, Berlin, Germany;*

18 *7 Berlin Institute of Health at Charité - Universitätsmedizin Berlin, Core Unit Bioinformatics, Berlin,*
19 *Germany;*

20 *8 Department of Congenital Heart Disease and Pediatric Cardiology, University Hospital of Schleswig-*
21 *Holstein, Kiel, Germany;*

22 *9 German Center for Cardiovascular Research (DZHK), Kiel, Germany;*

23 *10 Institute of Immunology and Genetics, Kaiserslautern, Germany;*

24 *11 Lipidomix GmbH, Berlin, Germany;*

25 *12 Institute of Computer-Assisted Cardiovascular Medicine, Charité - Universitätsmedizin Berlin,*
26 *corporate member of Freie Universität Berlin and Humboldt-Universität zu Berlin, Berlin, Germany*

27 *13 Harvard Medical School and Cardiovascular Division, Department of Medicine, Brigham and*
28 *Women's Hospital, Boston, USA;*

29 *14 Department of Pediatric Cardiology, Charité - Universitätsmedizin Berlin, corporate member of*
30 *Freie Universität Berlin and Humboldt-Universität zu Berlin, Berlin, Germany*

31
32 Correspondence to:
33 Jirko Kühnisch, PhD
34 Experimental and Clinical Research Center (ECRC),
35 a joint cooperation between the Charité Medical Faculty
36 and the Max Delbrück Center for Molecular Medicine (MDC),
37 Lindenberger Weg 80, 13125 Berlin, Germany
38 Phone: +4930 9406-3319, Fax: +49 30 9406-3358,
39 Email: jirko.kuehnisch@mdc-berlin.de
40
41 Sabine Klaassen, MD
42 Experimental and Clinical Research Center (ECRC),
43 a joint cooperation between the Charité Medical Faculty
44 and the Max Delbrück Center for Molecular Medicine (MDC),
45 Lindenberger Weg 80, 13125 Berlin, Germany
46 Phone: +4930 9406-3319, Fax: +49 30 9406-3358,
47 Email: klaassen@mdc-berlin.de
48
49

50   **Abstract**

51

52   **Background**: Mutation of the *PRDM16* gene has been associated with human

53   cardiomyopathy. The PRDM16 protein is a transcriptional regulator affecting cardiac

54   development via Tbx5 and Hand1 regulating myocardial structure. Biallelic *Prdm16*

55   inactivation induces severe cardiac dysfunction with postnatal lethality and hypertrophy in

56   mice. Early pathological events upon *Prdm16* inactivation have not been explored.

57

58   **Methods**: This study performed in depth pathophysiological and molecular analysis of male

59   and female *Prdm16$^{csp1/wt}$* mice carrying systemic, monoallelic *Prdm16* gene inactivation. We

60   systematically assessed early molecular changes with transcriptomics, proteomics, and

61   metabolomics. Kinetic modelling of the cardiac metabolism was undertaken *in silico* with

62   CARDIOKIN.

63

64   **Results**: *Prdm16$^{csp1/wt}$* mice are viable up to 8 months, develop hypoplastic hearts, and

65   diminished systolic performance that is more pronounced in female mice. *Prdm16$^{csp1/wt}$* hearts

66   demonstrate moderate alterations of specific transcripts and protein levels with consistent

67   upregulation of pyridine nucleotide-disulphide oxidoreductase domain 2 (Pyroxd2) and the

68   transcriptional regulator pre B-cell leukemia transcription factor interacting protein 1 (Pbxip1).

69   The strongest concordant transcriptional upregulation was detected for *Prdm16* itself

70   probably by an autoregulatory mechanism. *Prdm16$^{csp1/wt}$* cardiac tissue showed reduction of

71   metabolites associated with amino acid as well as glycerol metabolism, glycolysis, and

72   tricarboxylic acid cycle. Global lipid metabolism was also affected with accumulation of

73   triacylglycerides detected in male *Prdm16$^{csp1/wt}$* hearts. In addition, *Prdm16$^{csp1/wt}$* cardiac

74   tissue revealed diminished glutathione (GSH) and increased inosine monophosphate (IMP)

75   levels indicating oxidative stress and a dysregulated energetics, respectively. Metabolic

76   modelling *in silico* suggested lowered fatty acid utilization in male and reduced glucose

77   utilization in female *Prdm16$^{csp1/wt}$* cardiac tissue.

78

79   **Conclusions**: Monoallelic *Prdm16* mutation restricts cardiac performance in *Prdm16$^{csp1/wt}$*

80   mice. Metabolic alterations precede transcriptional dysregulation in *Prdm16$^{csp1/wt}$* cardiac

81   tissue. Female *Prdm16$^{csp1/wt}$* mice develop a more pronounced phenotype indicating a sexual

82   dimorphism at this early pathological window. This study suggests that metabolic

83   dysregulation is an early event in *PRDM16* associated cardiac pathology.

84
85

Novelty and Significance

What Is Known?
- Mutation of the *PRDM16* gene has been associated with human cardiomyopathy.
- Biallelic inactivation of *Prdm16* in mice induces severe cardiac dysfunction with early postnatal lethality.
- Prdm16 cooperates with transcription factors such as Tbx5 and Hand1 to activate transcriptional programs that define the development of the compacted myocardium.

What New Information Does This Article Contribute?
- Systemic, monoallelic inactivation in $Prdm16^{csp1/wt}$ mice induces cardiac dysfunction with normal survival.
- Metabolic alterations are the leading pathophysiological consequences and induce cardiac hypoplasia. On the molecular level this is associated with upregulation of metabolic regulators Pyroxd2 and Pbxip1.
- Metabolic response after *Prdm16* inactivation occurs in a sex specific manner.

Nonstandard Abbreviation and Acronyms

DCM	dilated cardiomyopathy
LVNC	left ventricular noncompaction cardiomyopathy
Pbxip1	pre B-cell leukemia transcription factor interacting protein 1
PRDM16	human PR/SET domain 16 gene
PRDM16	human PR/SET domain 16 protein
Prdm16	mouse PR/SET domain 16 gene
Prdm16	mouse PR/SET domain 16 protein
$Prdm16^{csp1/wt}$	mice carrying the csp1 mutant allele heterozygous
Pyroxd2	pyridine nucleotide-disulphide oxidoreductase domain 2

Background

Primary, genetically determined cardiomyopathies comprise a group of heterogenous cardiac diseases that eventually result in heart failure or arrhythmia. Approximately 100 genes have been linked to cardiomyopathy most frequently affecting the sarcomere, Z-disc, mitochondria, or ion channel regulation.[1,2] In addition to these disease circuits transcription and splicing may be disturbed in cardiomyopathy. The PR/SET domain 16 (PRDM16) protein is one such transcriptional regulator.[3] Mutation of the *PRDM16* gene causes dilated (DCM) and left ventricular noncompaction cardiomyopathy (LVNC) in patients.[4-7] Recently, rare variant association analysis linked LVNC to PRDM16 protein truncating variants.[8] Altogether, this suggests that *PRDM16* is a genetic factor critical for cardiac function either causing monogenic cardiomyopathy or other myocardial phenotypes.

Germline homozygous inactivation of *Prdm16* in *Prdm16$^{csp1/csp1}$* mice results in a complex phenotype involving several organs, cardiac hypoplasia, and early postnatal lethality.[9] More recently, the role of *Prdm16* in myocardial development and LVNC was assessed after homozygous, cardiac-specific *Prdm16* inactivation in *Xmlc2Cre;Prdm16$^{flox/flox}$* mice.[10] Homozygous *Xmlc2Cre;Prdm16$^{flox/flox}$* mice develop cardiac dysfunction and die prematurely before postnatal day 7. During cardiac development, Prdm16 cooperates with the transcription factors T-box 5 (Tbx5) and heart and neural crest derivatives expressed 1 (Hand1) to promote gene programs required for myocardial growth and compaction.[10] Prdm16 also suppresses neural gene expression.[10] Consequently, Prdm16 inactivation in *Xmlc2Cre;Prdm16$^{flox/flox}$* mice leads to biventricular hypertrabeculation and left ventricular dilatation.[10] Overall, this work established that *Prdm16* is critical for embryonic cardiac development and postnatal function, orchestrating the transcriptional circuits determining myocardial maturation.

Originally, PRDM16 was established as a determinant for differentiation, homeostasis, and function of brown/beige adipocytes.[11] PRDM16 induces gene programs for the development of brown adipocytes, represses muscle/white adipocyte specific genes, induces adaptive thermogenesis, and increases energy expenditure.[12-15] On a molecular level these effects are facilitated by physical interaction and coordination of key transcription factors such as peroxisome proliferator activated receptor alpha, gamma (PPARA, PPARG), mediator complex subunit 1 (MED1), or CCAAT enhancer binding protein delta (CEBPD).[12,16,17] Of note, a significant number of these PRDM16 associated proteins serve as critical regulators of fatty acid (FA) metabolism, glucose utilization, and/or cellular respiration.

This study tests the hypothesis that PRDM16 orchestrates cardiac metabolism and investigates its role beyond its known transcriptional functions in cardiac development and homeostasis. We characterize the heart of heterozygous *Prdm16$^{csp1/wt}$* mice in depth to

151 assess the impact of monoallelic germline *Prdm16* inactivation, as is present in patients with

152 *PRDM16* associated cardiomyopathy. We explore early molecular events upon *Prdm16*

153 inactivation and establish a preclinical animal model. *Prdm16$^{csp1/wt}$* mice show diminished

154 cardiac performance, normal survival, and altered body composition. Cardiac dysfunction is

155 explained on the molecular level by altered metabolism, redox balance, and FA/glucose

156 utilization. Overall, this study establishes heterozygous *Prdm16$^{csp1/wt}$* mice as a model for

157 early molecular pathomechanistic events in the development of the *PRDM16* associated

158 cardiomyopathy.

159

160

161 **Methods**

162 The high-throughput sequencing data and proteome data have been made publicly available
163 at the Gene Expression Omnibus (GEO accession No. …) and the Proteomics Identification
164 Database (PRIDE accession No. …). Other data and study materials are available from the
165 corresponding authors on reasonable request. Primer and antibodies used in this study are
166 available (Table I and II in the Data Supplement). A detailed material and methods section is
167 provided in the Supplemental Material. The *Prdm16$^{csp1/wt}$* mice (FVB.C-*Prdm16^{csp1}*/J) were
168 received from Jackson Laboratories, USA (JAX stock #013100). The FVB.C-*Prdm16^{csp1}*/J
169 strain was originally established by N-ethyl-N-nitrosourea (ENU) mutagenesis inducing a
170 missense C>A mutation at the intronic acceptor splice site of exon 7.[9] Maintenance,
171 physiological analysis and organ collection of *Prdm16$^{csp1/wt}$* mice was approved by the
172 Landesamt für Gesundheit und Soziales Berlin (LAGeSo), Germany (G0070/17).

173

174 **Results**

175 *Germline, heterozygous inactivation of Prdm16 induces mild cardiac dysfunction*

176 In human tissue RNA preparations *PRDM16* transcripts are most abundant in lung, followed

177 by aorta, adipose tissues, and heart (Figure 1A). Consistently, murine tissue RNA extracts

178 show approx. 10-fold higher *Prdm16* expression in lung compared to heart (Figure 1B).

179 Within different heart regions *Prdm16* shows abundant expression in the right ventricle (RV),

180 left ventricle (LV), and septum but not in the atria (Figure 1C). Potassium voltage-gated

181 channel member 4 (*Kcna4*) and myosin light chain 2 (*Myl2*) confirmed atrial and ventricular

182 origin, respectively. To assess clinically relevant physiological and molecular impact of

183 *Prdm16* in the heart, rather than the effects of biallelic *Prdm16* gene inactivation, we

184 analyzed heterozygous FVB.C-*Prdm16csp1*/J mice (*Prdm16csp1/wt*).[9] PCR genotyping and

185 Sanger sequencing confirmed presence of the c.888-3C>A (ENSMUSG00000039410)

186 variant on DNA level (Figure 1D, Figure I_A-B in the Data Supplement). To further validate

187 the impact of the *Prdm16* acceptor splice site variant c.888-3C>A

188 (ENSMUST00000030902.12) at the transcriptional level, we performed PCR and targeted

189 high throughput sequencing of total RNA isolated from different *Prdm16wt/wt* and *Prdm16csp1/wt*

190 tissues. These analyses suggest that the *Prdm16* acceptor splice site variant c.888-3C>A

191 affects mRNA splicing, produces several splice products, and the most abundant splice

192 products truncate Prdm16 proteins after approx. 340 amino acids (Figure 1E-F, for detailed

193 Results see Data Supplement).

194 Next, we tested *Prdm16* mutant transcript expression in the heart. *Prdm16* mutant transcripts

195 are ~40% diminished compared to controls using primer sets targeting the mutated exon6-8

196 region (Figure 1G, Figure I_F in the Data Supplement). In contrast, primer sets measuring

197 the overall *Prdm16* transcript level (exon3-4, exon14-15) detect increased expression in

198 *Prdm16csp1/wt* hearts. This suggests that *Prdm16* inactivation due to the c.888-3C>A variant

199 upregulates overall *Prdm16* mRNA expression. The Prdm16 protein level was assessed with

200 a mass spectrometry-based targeted proteomics approach, measuring and quantifying the

201 abundance of the peptide Prdm16_V875-K883 (Figure 1H). As expected, a ~50% reduction

202 of the Prdm16_V875-K883 level was observed in *Prdm16csp1/wt* lung compared to controls

203 (Figure 1I). In cardiac tissue the Prdm16_V875-K883 detection limit was not reached.

204 The survival of *Prdm16csp1/wt* mice is normal until 8 months (Figure 2A). Male and female

205 *Prdm16csp1/wt* mice exhibit body weight reduction by ~11% and ~20%, respectively (Figure

206 2B, Table III in the Data Supplement). In female *Prdm16csp1/wt* mice diminished body weight

207 was associated with reduced fat content (~14%) and increased relative muscle tissue content

208 (~8%). The absolute and relative heart weight is diminished in both male and female

209 *Prdm16csp1/wt* mice (Figure 2B). Transthoracic echocardiography was assed to characterize

210   the cardiac physiology of *Prdm16^csp1/wt^* mice. Echocardiography illustrates mild cardiac

211   hypoplasia and reduced systolic functional parameters such as stroke volume, cardiac

212   output, and ejection fraction (EF) (Figure 2C-D, Table IV-VI in the Data Supplement). Other

213   cardiac parameters such as heart rate, systolic/diastolic blood pressure, or electrophysiology

214   are unaffected in *Prdm16^csp1/wt^* mice. Cardiac tissue organization assessed by histology and

215   hematoxylin/eosin staining appeared normal in *Prdm16^csp1/wt^* hearts (Figure 2E). Fibrosis was

216   not detected, neither by Picro-Sirius red staining, nor by immunostaining of collagen 1 (Col1)

217   and alpha smooth muscle actin (αSma) (Figure 2F, Figure III in the Data Supplement).

218   Further analysis of *Prdm16^csp1/wt^* cardiac tissue with electron microscopy, morphometry,

219   quantitative PCR, and immunostaining identified no abnormalities of the sarcomere (Figure

220   IV in the Data Supplement, for detailed Results see Data Supplement). The relative

221   mitochondrial area in heart tissue was unaffected. Cardiomyocyte area was assessed

222   histomorphometrically in paraffin embedded heart tissue sections of comparable cross-

223   sectional level after wheat germ agglutinin (WGA) staining. Cardiomyocytes of female

224   *Prdm16^csp1/wt^* mice demonstrate significant reduction of cross-sectional area explaining

225   reduced myocardial mass (Figure 2G). Normal viability, myocardial hypoplasia, and

226   diminished cardiac performance due to monoallelic *Prdm16* inactivation suggests

227   *Prdm16^csp1/wt^* mice as a suitable model to explore early pathophysiological changes in

228   *PRDM16* associated cardiomyopathy.

229

230   *Moderate transcriptional dysregulation in Prdm16^csp1/wt^ hearts*

231   Prdm16 is a transcriptional regulator so we performed transcriptional profiling using RNAseq

232   of heart tissue comparing male and female *Prdm16^csp1/wt^* mice with corresponding controls.

233   Comparing female to male control heart tissue, we found 51 up-regulated and 92 down-

234   regulated genes, applying an absolute log2 fold change (LFC) threshold >0.5 (Figure 3A).

235   Male *Prdm16^csp1/wt^* mice showed 12 up-regulated and 16 down-regulated genes compared to

236   male controls. Female *Prdm16^csp1/wt^* mice revealed 55 up-regulated and 35 down-regulated

237   genes, respectively. Transcriptional profiling identified most significant up-regulation of

238   *Prdm16* in males and females suggesting an autoregulatory control of expression (Figure 3B-

239   C). Other transcripts of the PRDM gene family were not regulated (Figure V_A-B in the Data

240   Supplement).

241   Next, the top 20 up- and down-regulated genes for males and females were evaluated. In

242   male *Prdm16^csp1/wt^* mice we observed upregulation for MBL associated serine protease 2

243   (*Masp2*), synapsin II (*Syn2*) a coat protein of clathrin-coated vesicles, and UbiA

244   prenyltransferase domain containing 1 (*Ubiad1*) controlling coenzyme Q10 synthesis (Figure

245   3D). We detected decreased levels of transcripts for synuclein alpha (*Snca*), hemoglobin

246　alpha adult chain 1 (*Hba-a1*), and hemoglobin subunit beta (*Hbb-ba*), which both
247　supply/control intracellular oxygen. Female *Prdm16^csp1/wt* cardiac tissue showed up-regulation
248　of the extra cellular matrix CUB domain containing protein 1 (*Cdcp1*), ladinin (*Lad1*) involved
249　in basement membrane organization, the cell adhesion protein spondin 2 (*Spon2*), nuclear
250　receptor subfamily 1, group D, member 1 (*Nr1d1*) a transcriptional repressor coordinating
251　metabolic pathways, and nicotinamide riboside kinase 2 (*Nmrk2*) regulating laminin matrix
252　deposition. Aldehyde dehydrogenase family 3, subfamily A1 (*Aldh3a1*) and gastrokine 3
253　(*Gkn3*) showed strongest down-regulation in female *Prdm16^csp1/wt* cardiac tissue. The top 20
254　genes were tested for their cellular expression in heart tissue (www.proteinatlas.org). Most
255　genes showed a broad expression in cardiomyocytes, endothelial cells, fibroblasts, immune
256　cells, and smooth muscle cells. Thus, no enrichment of cell lineage specific genes was
257　found. The majority of dysregulated genes in male and female *Prdm16^csp1/wt* cardiac tissue
258　are associated with transcription (T), metabolism (M), and indirect/direct immune response
259　(I).

260　Concordant and discordant changes in males vs. females were assessed with LFC
261　significance threshold of >0.25 and <-0.25, respectively. Strongest concordant up-regulated
262　genes in *Prdm16^csp1/wt* hearts were *Prdm16*, *Lad1*, *Ubiad1*, and the pre B-cell leukemia
263　transcription factor interacting protein 1 (*Pbxip1*) (Figure 3E). Systematic dysregulation of
264　critical cardiac genes was tested using the harmonizome gene set *congenital heart disease*.
265　Evaluation did not identify consistent, significant dysregulation of cardiac specific transcripts
266　(Figure V_C in the Data Supplement). Differentially expressed genes from *Prdm16^csp1/wt*
267　hearts (TOP5 up- and down-regulated genes) and known PRDM16 interacting genes
268　(physical interaction, transcriptional targets, transcriptional complex component) were tested
269　for dysregulation in a human DCM patients dataset.[18] From more than 60 known PRDM16
270　targets *PPARA*, *MED1*, and *CEBPD* were dysregulated in the human DCM screen (Table VII
271　in the Data Supplement). Moreover, the chemotactic factor 2 (*Ccl2*) was dysregulated in
272　DCM patients and in male *Prdm16^csp1/wt* mice. Sex specific gene expression validated correct
273　technical procedures of RNAseq *Prdm16^csp1/wt* mice analysis (Figure V_D in the Data
274　Supplement). Next, we generated a gene ontology (GO) network using the male and female
275　TOP20 up- and down-regulated genes in *Prdm16^csp1/wt* hearts (GOnet).[19] Strongest functional
276　association of dysregulated genes in *Prdm16^csp1/wt* hearts was found for the GO terms
277　*response to lipids* and *response to oxygen-containing compounds* (Figure 3F, Figure V_E in
278　the Data Supplement). Thus, *Prdm16^csp1/wt* hearts show moderate, sex specific transcriptional
279　dysregulation with the strongest regulated transcripts being *Prdm16*, *Lad1*, *Ubiad1*, and
280　*Pbxip1.* GO and individual transcript evaluation suggest an impact on metabolic processes
281　after monoallelic *Prdm16* inactivation.

282

283   *Proteome analysis of Prdm16^{csp1/wt} hearts reveals upregulation of Pbxip1 and Pyroxd2*

284   In order to verify findings from the transcriptional analysis and to assess cardiac tissue

285   protein expression, we performed a global proteomic analysis of cardiac tissue. Consistent

286   with RNAseq, male *Prdm16^{csp1/wt}* cardiac tissue showed less variation from control than

287   female samples. Of the 3,847 proteins identified in total, 3,314 were used for quantitation.

288   Sample identity was confirmed by expression level of the male-specific DEAD box helicase

289   3, Y-linked (Ddx3y) and eukaryotic translation initiation factor 2, subunit 3, structural gene Y-

290   linked (Eif2s3y). The Prdm16 protein was not detected, which can be explained by very low

291   abundance below the limit of detection. Most significant differences in protein expression

292   were observed between male and female cardiac tissue (165 proteins with FDR <5%, data

293   not shown). Pairwise evaluation of control and *Prdm16^{csp1/wt}* proteome data from male

294   cardiac tissue using a p-value cutoff 0.01 showed upregulation of fermitin family member 2

295   (Fermt2), coatomer protein complex, subunit zeta 2 (Copz2), and pyridine nucleotide-

296   disulphide oxidoreductase domain 2 (Pyroxd2) (Figure 4A). Substantial downregulation was

297   observed for c-src tyrosine kinase (Csk), translocase of inner mitochondrial membrane 10B

298   (Timm10b), and collagen type XVIII, alpha 1 (Col18a1) proteins. Pairwise evaluation of

299   proteome data from female cardiac tissue showed strongest upregulation of Pyroxd2,

300   pyruvate dehydrogenase kinase, isoenzyme 4 (Pdk4), and pre B cell leukemia transcription

301   factor interacting protein 1 (Pbxip1) in *Prdm16^{csp1/wt}* mice (Figure 4B). Strongest

302   downregulation was detected for cystic fibrosis transmembrane conductance regulator (Cftr),

303   WNK lysine deficient protein kinase 1 (Wnk1), and huntingtin interacting protein 1 (Hip1).

304   To further assess *Prdm16* genotype driven differences, we performed also pairwise

305   evaluation of combined male and female groups (p-value cutoff 0.01). In total we identified

306   53 up- or downregulated proteins (Figure 4C, Figure VI in the Data Supplement). Pyroxd2,

307   Pbxip1, and ribosomal protein L30 (Rpl30) appeared as the strongest concordantly

308   upregulated proteins in *Prdm16^{csp1/wt}* cardiac tissue. Furthermore, the strongest concordant

309   downregulation was found for Cftr, Col18a1, and hexokinase 1 (Hk1) in *Prdm16^{csp1/wt}* cardiac

310   tissue. By adding an additional filter (abs log2 ratio >0.5), the top regulated proteins (n=18)

311   were selected (Figure 4D). Among these, Pyroxd2 and Pbxip1 represent the two most

312   significantly regulated candidates in *Prdm16^{csp1/wt}* cardiac tissue (p-value<0.0001). Pyroxd2 is

313   a critical regulator of hepatic mitochondrial function, interacts with mitochondrial complex IV,

314   and appears consistently upregulated in *Prdm16^{csp1/wt}* hearts on transcript as well as protein

315   level.[20] Pbxip1 interacts with transport as well as regulatory proteins and indirectly affects

316   transcription.[21] Proteome data did not show differential expression of mitochondrial transport

317   proteins and respiratory chain complexes (Figure VII in the Data Supplement). Proteome

318   data for sarcomere components, glycolysis, and amino acid metabolism did not show

319   differential expression (Figure VIII in the Data Supplement). Altogether protein expression

320 analysis identifies specific dysregulation of the mitochondrial protein Pyroxd2 and the
321 transcriptional regulator Pbxip1.

322

323 *Altered metabolism in Prdm16$^{csp1/wt}$ cardiac tissue*

324 As expression analysis pointed towards a metabolic impact of Prdm16 in cardiac tissue, we
325 also analyzed central carbon metabolites in *Prdm16$^{csp1/wt}$* cardiac tissue with gas
326 chromatography mass spectrometry (GC-MS). Measured values are presented as log2 from
327 ratio of mean of the normalized peak areas *Prdm16$^{csp1/wt}$*/controls (values >0.2, blue and
328 values <-0.2, red). Overall, we detected several diminished metabolites (log2 ratios
329 *Prdm16$^{csp1/wt}$*/controls) for all assessed metabolic processes (Figure 5A). In *Prdm16$^{csp1/wt}$*
330 cardiac tissue, amino acid, glycerol, pentose phosphate pathway (PPP), glycolysis,
331 tricarboxylic acid cycle (TCA), and nucleobase metabolism were all reduced. Individual
332 metabolite analysis of female *Prdm16$^{csp1/wt}$* cardiac tissue revealed statistically significant
333 reductions for glycerol-3-phosphate, phosphoenolpyruvic acid, succinic acid, and 3-hydroxy
334 butanoic acid. Combined female and male cardiac tissue analysis identified significant
335 reduction of phosphoenolpyruvic acid, pyruvic acid, and ribose-5-phosphate in *Prdm16$^{csp1/wt}$*
336 hearts. As interpretation of individual metabolites is difficult, we assessed the designated
337 pathway profiles of central carbon metabolites with univariate analysis. Univariate analysis
338 counts each increased/diminished metabolite as ordinary number. Combined pathways
339 analysis using female and male values identified significant reduction of amino acid,
340 glycolysis, glycerol, and TCA metabolism in *Prdm16$^{csp1/wt}$* hearts (Figure 5B).

341 The adult heart mainly relies on FA oxidation as its primary substrate, so we next explored
342 lipid metabolism with liquid chromatography-mass spectrometry (LC-MS) in depth. Values
343 are presented as log2 from ratio *Prdm16$^{csp1/wt}$*/controls (values >0.2, blue and values <-0.2,
344 red). Evaluation of lipid classes did not reveal significant dysregulation. The strongest
345 alterations were observed in male *Prdm16$^{csp1/wt}$* hearts for triacylglycerol compounds (TAG;
346 increase), dihydroceramides (DCER; reduction), and hexosylceramides (HCER; reduction)
347 (Figure 5C). Currently, there is little known about dysregulation of individual lipid classes in
348 early cardiac dysfunction.[22,23] Individual lipids are presented as log2 of ratio
349 *Prdm16$^{csp1/wt}$*/controls. Although accumulated lipid classes appear widely normal a minority of
350 individual lipids were dysregulated (Figure IX_A in the Data Supplement). Important FA such
351 as oleic, linoleic, α-linolenic, and arachidonic acid show moderate alteration (Figure 5D).
352 Several diacylglycerols (DAG) appear strongly reduced in *Prdm16$^{csp1/wt}$* hearts for instance
353 DAG(16:1/18:0), which was altered in a study assessing lipid profiles in human heart
354 failure.[23] DAG(18:1/20:4), which was significantly altered on lipidomic profiling of murine
355 hearts after exercise or pressure overload, was normal in *Prdm16$^{csp1/wt}$* hearts.[22] Enrichment

356   of individual TAG was significant for TAG47:2-FA18:2, TAG50:4-FA20:4, and TAG51:4-

357   FA18:3 in male and to lesser degree in female *Prdm16^{csp1/wt}* cardiac tissue. The sphingolipids

358   sphingomyelin SM(14:0), dihydroceramide DCER(16:0), and ceramide CER(22:1) show

359   strongest reduction in male *Prdm16^{csp1/wt}* cardiac tissue. The hexosylceramide,

360   HCER(d18:1/16:0) appeared diminished in hearts of both *Prdm16^{csp1/wt}* sexes. Several

361   protective and risk predictive sphingolipids identified by *Wittenbecher et al.* [23] were

362   unaffected in *Prdm16^{csp1/wt}* mice. The global levels of the cardiac phospholipids

363   phosphatidylcholine (PC) and phosphatidylethanolamine (PE) were unaffected (Figure 5C).

364   Individual PC and PE species appeared consistently enhanced (e.g. PC(18:2/18:3),

365   PE(17:0/22:5), PE(P-18:0/18:0)) or decreased (e.g. PC(18:1/16:1), PE(P-18:1/18:1), PE(P-

366   18:1/18:2)) in *Prdm16^{csp1/wt}* hearts of both sexes (Figure IX_B in the Data Supplement). The

367   level of cardiolipin (CA(18:2(4)), a phospholipid critical for mitochondrial function, appeared

368   moderately elevated in male *Prdm16^{csp1/wt}* hearts (Figure 5D). Thus, global lipid metabolism

369   is altered in male *Prdm16^{csp1/wt}* hearts with accumulation of TAG.

370   Cardiac metabolism is controlled by the mitogen-activated protein kinase (MAPK) and

371   mechanistic target of Rapamycin (mTOR) pathways. Using the Milliplex phosphoprotein

372   magnetic bead system we tested the phosphorylation level of key proteins from relevant

373   pathways. Female *Prdm16^{csp1/wt}* hearts showed significant inactivation of insulin receptor

374   (Insr_Tyr1162-1163), phosphatase and tensin homolog (Pten_Ser380), and Akt

375   serine/threonine kinase 2 (Akt_Ser473) phosphorylation (Figure 5E). mTOR phosphorylation

376   activation at Mtor_Ser2448 and tuberin (Tsc2_Ser939) showed increased phosphorylation

377   without reaching statistical significance. Thus, diminished phosphorylation of the Insr/Akt

378   pathway activates mTOR signaling and cardiac metabolism adapts accordingly. Altogether,

379   *Prdm16^{csp1/wt}* hearts show multiple, substantial metabolic alterations suggesting that

380   monoallelic *Prdm16* inactivation affects cardiac metabolism.

381

382   *Tissue energetics and production of protective lipids in Prdm16^{csp1/wt} hearts*

383   To further explore the consequences of the imbalanced cardiac metabolism in *Prdm16^{csp1/wt}*

384   mice, we tested the steady-state levels of important cardiac metabolic intermediates, redox

385   molecules, and eicosanoids. Global adenosine triphosphate (ATP) levels were unaffected in

386   *Prdm16^{csp1/wt}* cardiac tissue (Figure 6A, Table VIII in the Data Supplement). However, the

387   ratio of adenosine monophosphate to ATP (AMP/ATP) was significantly increased in female

388   *Prdm16^{csp1/wt}* hearts. AMP is a critical molecule for sensing metabolic stress conditions and

389   the increased AMP/ATP ratio suggests an abnormal energy state in the *Prdm16^{csp1/wt}* cardiac

390   tissue. We also detected increased absolute and relative inosine monophosphate (IMP)

391   values in both male and female *Prdm16^{csp1/wt}* hearts (Figure 6B). IMP is the key molecule in

392   purine metabolism and a sensitive measure of the ATP turnover.[24] The level of hypoxanthine,

393   which serves as precursor and degradation product of IMP, was elevated in male

394   *Prdm16[csp1/wt]* hearts. The ratio of reduced to oxidized nicotinamide adenine dinucleotide

395   (NADH/NAD+), serving as central hydride donor for oxidative phosphorylation and in many

396   other redox reactions[25], was increased in female *Prdm16[csp1/wt]* hearts (Figure 6C). The ratio

397   of reduced to oxidized glutathione (GSH/GSSG) was diminished in female *Prdm16[csp1/wt]*

398   hearts suggesting accelerated cellular GSH consumption and redox imbalance (Figure 6D).

399   The levels of creatine, phosphor-creatine/creatine, and acetyl-CoA appeared normal. The

400   level of 4-hydroxynonenal (4-HNE), a marker of lipid peroxidation, was unaffected. These

401   findings suggest accelerated ATP turnover and oxidative stress but no lipid peroxidation on

402   *Prdm16* inactivation in particular in female *Prdm16[csp1/wt]* hearts.

403   Apart from their function as nutritional source FA serve as reactant for biosynthesis of

404   hydroxyeicosatetraenoic acids (HETE) and epoxyeicosatrienoic acids (EET)[26,27]. All HETE

405   species, which are synthesized from arachidonic acid, FA(20:4) by lipoxygenases (LOX),

406   were normal in male *Prdm16[csp1/wt]* cardiac tissue (Figure 6E, Table IX in the Data

407   Supplement). 20-HETE, which is synthesized from FA(20:4) by cytochrome P450 (CYP), was

408   also unaffected. All tested individual EET, which originate from CYP activity, and summed

409   EET were significantly increased. Consistently, also the water soluble

410   dihydroxyeicosatrienoic acids (DHET), representing the corresponding EET hydrolyzation

411   products, were significantly increased. The anti-inflammatory 19,20-epoxydocosapentaenoic

412   acid (19,20-EDP) and 17,18-epoxyeicosatetraenoic acid (17,18-EEQ) were also significantly

413   increased. These observations suggest activation of CYP mediated bioactive, lipid

414   production (EETs and 19,20-EDP) in male *Prdm16[csp1/wt]* cardiac tissue.

415   To assess the global metabolism of *Prdm16[csp1/wt]* cardiac tissue, we modelled major

416   metabolic pathways with CARDIOKIN1 *in silico*. As input data we used quantitative protein

417   expression data of metabolically important proteins measured with LC-MS/MS (Figure 4).

418   The calculated maximal utilization rates of the given metabolic condition are upper estimates

419   that will probably not be reached under physiological conditions. However, these maximal

420   utilization rates allow estimation of the physiological capacity. The maximal FA and glucose

421   utilization rates were different between cardiac the tissue of male and female control hearts.

422   Females had lower FA but higher glucose utilization capacity compared to male controls

423   (Figure 6F). In addition, the maximal lactate utilization rate was lower in female controls. In

424   male *Prdm16[csp1/wt]* cardiac tissue the maximal FA utilization was decreased but unaffected in

425   females. In contrast, female *Prdm16[csp1/wt]* cardiac tissue had a diminished maximal glucose

426   utilization, while the males were unaffected. Maximal lactate utilization was increased in

427   female *Prdm16[csp1/wt]* cardiac tissue. Maximal ATP production and O_2 consumption were

428   modelled under fasting and postprandial conditions. Under both conditions the cardiac tissue

429   of female controls showed diminished maximal ATP production and O_2 consumption

430   compared to male controls (Figure X in the Data Supplement). The maximal utilization rate

431   gives a net measure involving several members of the given metabolic pathway. Thus, we

432   aimed to identify enzymes critical for FA and glucose metabolism in $Prdm16^{csp1/wt}$ cardiac

433   tissue. For this purpose, the metabolic utilization and protein abundance was correlated for

434   each protein and animal. The strongest correlations, indicated by low p-values, were

435   identified for carnitine palmitoyltransferase 2 (Cpt2), acetyl-CoA acyltransferase 2 (Acaa2),

436   hexokinase 1 (Hk1), and others (Figure 6G, Figure XI in the Data Supplement). In controls,

437   Cpt2 and Acaa2, two determinants of the mitochondrial beta-oxidation activity, showed lower

438   maximal capacity in females supporting their diminished FA metabolism (Figure 6G, Figure

439   XII in the Data Supplement). Lower Cpt2 capacity in male $Prdm16^{csp1/wt}$ cardiac tissue partly

440   explains diminished male FA metabolism. Consistent with protein expression data, female

441   and male $Prdm16^{csp1/wt}$ cardiac tissue showed diminished Hk1 utilization. Hk1 mediates

442   phosphorylation of D-glucose to D-glucose 6-phosphate and represents the initial step of

443   glycolysis. Altogether, these findings support imbalanced substrate metabolism and oxidative

444   stress on monoallelic $Prdm16$ inactivation.

Discussion

445   Our study suggests that metabolic dysregulation is an early event in *Prdm16* associated

446   cardiac dysfunction and precedes substantial transcriptional dysregulation. Metabolic

447

448   changes upon *Prdm16* inactivation appear to contribute to induce early and late-stage

449   cardiac pathologies, which may result in cardiac hypoplasia[9] and hypertrophy[28], respectively.

450   Pyroxd2 and Pbxip1 are novel modulators of cardiac function, reflecting the central role of

451   metabolism in the *Prdm16* associated cardiac phenotype. Moreover, our study detects a

452   more pronounced molecular and structural phenotype in *Prdm16*[csp1/wt] females than males,

453   with sex having a larger effect than the *Prdm16* genotype. The differential response in

454   maximal FA and glucose utilization of male and female *Prdm16*[csp1/wt] hearts suggest a

455   diminished capacity of females to scope with metabolic challenges.

456

457   *PRDM16 cardiomyopathy.*

458   Mutation of *PRDM16* is a cause of cardiomyopathy associated with DCM and LVNC.[4] More

459   recently, truncating variants in *PRDM16* were identified by *in silico* analysis as one of three

460   specific LVNC variant classes.[8] These genetic observations and the *Prdm16*[csp1/wt] phenotype

461   reinforce the human genetic case that heterozygous *PRDM16* inactivation/truncation is

462   sufficient to cause cardiomyopathy. Functional evidence from *Prdm16*[csp1/wt] mice, mirroring

463   the genotype of patients with *PRDM16* mutation, will increase the ClinGen evidence from

464   *limited* to *moderate* for the association of *PRDM16* with cardiomyopathy

465   (www.clinicalgenome.org).

466   In mice, homozygous *Prdm16* inactivation induces discordant phenotypes in different genetic

467   backgrounds resulting in either early postnatal lethality (*Xmlc2Cre;Prdm16*[flox/flox]) or cardiac

468   dysfunction with fibrosis at adult stages (*Mesp1Cre;Prdm16*[flox/flox],

469   *Myh6Cre;Prdm16*[flox/flox]).[10,28,29] *Xmlc2Cre* and *Mesp1Cre* strains are expected to inactivate

470   *Prdm16* upon very early heart development.[30] Discrepancies in penetrance of the

471   phenotypes could be attributed to incomplete spatial Cre-mediated *Prdm16* inactivation and

472   residual Prdm16 levels in early cardiomyocyte progenitor cells, endothelia, or cardiac

473   fibroblasts. Consistent with neuronal studies, it is likely that *Prdm16* has additional effects on

474   cardiac stem and progenitor cell function compared with differentiated, adult

475   cardiomyocytes.[31] Indeed, adult *Prdm16* inactivation using a tamoxifen-inducible mouse

476   model *(αMHC-MerCreMer;Prdm16*[flox/flox]) resulted in viable mice without an overt cardiac

477   phenotype.[10] Homozygous *PRDM16* mutation has not been identified in patients so far but

478   based on animal studies[10,28,29], biallelic *PRDM16* inactivation likely induces a highly

479   penetrant, severe cardiac phenotype in humans that may not survive to birth. In *Prdm16*[csp1/wt]

480   hearts we did not observe alterations in myocardial compaction or alterations of the gene

481   circuit involving Tbx5 and Hand1.[10] This is possibly due to the heterozygous nature of the

482   *Prdm16* inactivation in our model. Another important feature is that *Prdm16*[csp1/wt] hearts do

483   not show perturbation of the sarcomere at either a structural or a molecular level. This

484   suggests that contractile dysfunction in the *PRDM16* cardiomyopathy originates from other

485   mechanisms such as energy restriction or metabolic stress affecting contractility and/or ion

486   homeostasis.

487

488   *Prdm16 differentially compromises metabolism in early and late stage cardiac pathology.*

489   Studies from adipose tissue show that PRDM16 orchestrates adipocyte differentiation via

490   interaction with proteins such as PPARA, PPARG, MED1, CEBPD, peroxisome proliferator-

491   activated receptor gamma coactivator 1-alpha, beta (PPARGC1A, PPARGC1B), or

492   uncoupling protein 1 (UCP1).[3,12,13,15-17,32,33] Consequently, we explored a selection of

493   validated PRDM16 targets in *Prdm16*[csp1/wt] hearts and in a transcriptomic screen of human

494   adult DCM (Table VII in the Data Supplement).[18] We found only three PRDM16 targets,

495   namely PPARA, MED1, and CEBPD dysregulated in this DCM transcriptomic screen.

496   Moreover, the transcriptional targets Tbx5, Hand1 identified in *Xmlc2Cre;Prdm16*[flox/flox] hearts

497   appeared not be regulated in *Prdm16*[csp1/wt] hearts.[10] This suggests: *i)* in cardiomyocytes

498   PRDM16 steers diverse regulatory programs compared to other differentiated cell types, *ii)*

499   expression changes are time sensitive and depend on the progenitor or differentiation stage,

500   and *iii)* early molecular changes or adaptations in PRDM16 cardiac pathology are not

501   associated with broad, significant expression changes. In the absence of major

502   transcriptional effects in our model, we investigated possible metabolic alterations.

503   The initial evidence that metabolic alteration may be associated with the cardiac *PRDM16*

504   phenotype came from a study analyzing homozygous *Mesp1Cre;Prdm16*[flox/flox] mice. These

505   mice develop cardiac hypertrophy, diminished heart function, fibrosis, reduced mitochondrial

506   content, and diminished acylcarnitine levels at 12 months of age.[28] *Mesp1Cre;Prdm16*[flox/flox]

507   hearts show upregulation of transcripts involved in glucose metabolism, transcriptional

508   downregulation of lipid metabolism, and oxidative stress gene expression. Metabolic high-fat

509   diet challenge of young *Mesp1Cre;Prdm16*[flox/flox] mice induced cardiac dysfunction as well as

510   hypertrophy already at 3 months of age compared to a later phenotype onset at 9 months

511   without high-fat diet. This suggests that complete *Prdm16* inactivation in the heart leads to

512   diminished mitochondrial volume and sensitivity to substrate availability ultimately resulting in

513   cardiomyocyte hypertrophy by activating distinctive gene programs.[28] Exploration of the heart

514   phenotype in *Xmlc2Cre;Prdm16*[flox/flox] mice also detected downregulation of transcripts

515   associated with mitochondrial biogenesis/function and FA metabolism.[10] Together, both

516 models analyzing homozygous *Prdm16* inactivation demonstrate cardiac phenotypes that are
517 associated with diminished metabolic capacity eventually leading to cardiac growth and
518 hypertrophy. In contrast, heterozygous *Prdm16^csp1/wt* hearts are hypoplastic with no evidence
519 of mitochondrial volume changes, demonstrating that metabolic alterations are early events
520 in *Prdm16* inactivation.

521 A differential response in maximal FA or glucose utilization of male and female *Prdm16^csp1/wt*
522 is supported by sex-specific transcriptional dysregulation. In male *Prdm16^csp1/wt* hearts the
523 strongest up- and downregulation was observed for *Ubiad1* and hemoglobin's (*Hba-a1*, *Hbb-*
524 *bs*), respectively. Ubiad1 is a prenyltransferase that is involved in ubiquinone (CoQ10)
525 synthesis, thus, increasing redox tolerance and providing cardiovascular protection.[34]
526 Cellular downregulation of Hba-a1 and Hbb-ba diminishes oxygen supply and may blunt
527 cardiac oxidative stress in the setting of restricted FA oxidation. Female *Prdm16^csp1/wt* hearts
528 show strongest up- and downregulation of the metabolism associated transcripts *Nr1d1* and
529 *Aldh3a1*, respectively. NR1D1 is a ligand-regulated transcriptional repressor impacting
530 metabolic regulation, cellular differentiation, or circadian rhythm control.[35] Upon
531 adipogenesis, *Nr1d1* gene silencing affects brown adipocyte differentiation and attenuates
532 *Prdm16* expression suggesting an interaction of both.[35] A recent study exploring the impact
533 of shift work on cardiac reperfusion injury demonstrated diminished myocardial Nr1d1
534 expression suggesting a more general role of Nr1d1 in cardiomyocyte function.[36] Aldh3a1 is
535 involved in oxidation and detoxification of lipid peroxids. Genetic inactivation of *Aldh3a1* in
536 zebrafish increases 4-HNE levels and impairs glucose homeostasis.[37] Thus, Aldh3a1
537 reduction is likely associated with metabolic adaptation of female *Prdm16^csp1/wt* glucose
538 utilization. Overall, early transcriptional changes in *Prdm16^csp1/wt* hearts are distinct from
539 those observed in later stage pathology.

540

541 *Pyroxd2 and Pbxip1 are novel modulators of cardiac function.*

542 In line with a central role of metabolism for PRDM16-associated cardiac phenotypes, we
543 found concordant upregulation of Pyroxd2 and Pbxip1 both of which have been implicated in
544 the regulation of energy metabolism. PBXIP1 interacts with several proteins such as the
545 transcription factor Pre-B cell leukemia factor 1 (PBX1)[38], microtubules[38], estrogen receptors
546 1 and 2 (ESR1, ESR2)[39], and AMP-activated protein kinase (AMPK).[40] Moreover, PBXIP1
547 regulates the activity of MAPK and mTOR signaling.[21] The function of Pbxip1 in the heart is
548 largely unknown. In a prior genetic screen, the inhibition of MAPK signaling pathway proteins
549 increased PBXIP1 phosphorylation.[41] In contrast, activation of the MAPK signaling cascade
550 increased PBXIP1 protein expression and murine PBXIP1 overexpression stimulated cardiac
551 hypertrophy.[41] In *Prdm16^csp1/wt* hearts we found Pbxip1 upregulation associated with

552 diminished MAPK signaling activity. Mutation of *PBXIP1* has not been associated with
553 human heart disease; however, mutation of its interacting transcription factor PBX1 has been
554 linked to syndromic congenital heart defects.[42] An interesting aspect of PBXIP1 is its
555 interaction and activation of ESR1 and ESR2, a potential mechanisms of sex specific
556 effects.[39] Our data implicate PBXIP1 in cardiac growth, metabolism, and hypertrophy which
557 await further characterization under healthy and diseased conditions. In the context of
558 *Prdm16* heterozygous mutants, Pbxip1 may orchestrate the adaptive responses of important
559 signaling cascades like AMPK, mTOR, or MAPK.

560 The cardiac function of Pyroxd2 is unknown. PYROXD2 is an oxidoreductase of the inner
561 mitochondrial membrane/matrix that interacts with mitochondrial complex IV.[20] Genetic
562 inactivation of PYROXD2 in hepatic cell lines decreased the mitochondrial membrane
563 potential, complex IV activity, ATP content, and mitochondrial DNA copy number.[20]
564 PYROXD2 inactivation also increased mitochondrial reactive oxygen species and the
565 number of immature mitochondria.[20] Compound heterozygous genetic variants in *PYROXD2*
566 were detected in a single patient with a severe infantile metabolic disorder.[43] Molecular
567 workup in patient fibroblasts demonstrated a mito-ribosomal defect characterized by
568 increased mitochondrial superoxide levels, elevated sensitivity to metabolic stress,
569 decreased complex I subunit proteins, and diminished mitochondrial ribosome levels.[43]
570 Mutation of a related human oxidoreductase, *PYROXD1*, results in early-onset skeletal
571 myopathy.[44] Another study, investigating molecular signatures in skeletal muscle from heart
572 failure patients, detected upregulation of *PYROXD2* transcripts.[45] These data suggest that
573 Pyroxd2 upregulation in *Prdm16*$^{csp1/wt}$ hearts may compensate for metabolic and oxidative
574 stress conditions.

575

576 *Sex specific aspects of Prdm16 inactivation in cardiac metabolism.*

577 Our study detects a more pronounced cardiac and molecular phenotype in *Prdm16*$^{csp1/wt}$
578 females compared to males. The original cytogenetic association of *PRDM16* inactivation
579 with cardiomyopathy was described in 18 patients with 1p36 syndrome.[4] Among these, 16
580 individuals were females and only two were males.[4] This may point to a sex specific
581 penetrance of the *PRDM16* cardiomyopathy. Apparently, female *Prdm16*$^{csp1/wt}$ mice
582 compensate the cardiac metabolic disturbance less efficiently than males. Metabolic
583 modelling with CARDIOKIN1 revealed diminished FA, increased glucose, and reduced
584 lactate utilization in the hearts of female compared with male *Prdm16*$^{wt/wt}$ mice.[46] This
585 establishes clear sexual dimorphism for cardiac metabolism under basal healthy conditions.[47]
586 Under normal conditions the heart generates ATP mainly via FA oxidation and glucose
587 utilization (glycolysis, pyruvate supply to TCA).[48] Female *Prdm16*$^{csp1/wt}$ hearts show

588   diminished maximal glucose and unaffected FA utilization. The increase in the maximal

589   lactate utilization capacity in female $Prdm16^{csp1/wt}$ hearts likely reflects an adaptation to

590   metabolic stress conditions. Male $Prdm16^{csp1/wt}$ hearts show diminished maximal FA

591   utilization, which is in line with the TAG accumulation we observed. Male $Prdm16^{csp1/wt}$ hearts

592   expose elevated EET levels, which is in line with a recent study demonstrating increased

593   EET levels/turnover in LV biopsies from DCM patients.[49] This supports distinct mechanisms

594   of lipid metabolism in male hearts. Whether hormonal differences are the cause of

595   systemically reduced fat content and the more advanced pathology in female $Prdm16^{csp1/wt}$

596   mice is unclear. The known association of Pbxip1 and Esr1/Esr2 activity as well as Nr1d1

597   provides a potential explanation for the sexual dimorphism in the regulation of substrate

598   utilization. Transcript as well as protein level of $Prdm16^{csp1/wt}$ hearts demonstrate significant

599   sex effects. Indeed, sex has a larger effect on metabolic parameters than the $Prdm16$

600   genotype at least during this investigated early pathological window. Our findings suggest a

601   sexual dimorphism for the $PRDM16$ associated cardiomyopathy with probably earlier, more

602   penetrant phenotype expression in females.

603 **Study Limitations**

604 Female *Prdm16*^{csp1/wt} mice have diminished relative total body fat content and increased

605 relative muscle content. This mirrors either the female tissue specific metabolism and/or

606 points towards a systemic factor affecting tissue development. Identification of such factor

607 would be important to understand the systemic (endocrine) role of Prdm16 and to test

608 therapeutic approaches targeting adipose tissue. Our study does not assess early metabolic

609 changes in cardiac progenitor cells. Analysis of *Prdm16*^{csp1/wt} hearts with *in silico* tools and

610 individual metabolite measurements suggest an accelerated metabolism. However, we did

611 not perform kinetic experiments to demonstrate accelerated turnover of selected metabolic

612 pathways.

Acknowledgments

Sources of Funding

Disclosures

All authors declare to have no conflict of interest related to this manuscript.

ORCID
Berndt, Nikolaus - https://orcid.org/0000-0001-5594-9940
Beule, Dieter - https://orcid.org/0000-0002-3284-0632
Dartsch, Josephine - https://orcid.org/0000-0002-7947-2881
Fritsche-Guenther, Raphaela - https://orcid.org/0000-0002-6965-0226
Heuser, Arnd - https://orcid.org/0000-0002-3334-960X
Huebner, Norbert - https://orcid.org/0000-0002-1218-6223
Kahlert, Anne-Karin - https://orcid.org/0000-0002-3201-2642
Kirchner, Marieluise - https://orcid.org/0000-0002-7049-534X
Kirwan, Jennifer - https://orcid.org/0000-0002-5423-1651
Klaassen, Sabine - https://orcid.org/0000-0001-5925-9912
Kühnisch, Jirko - https://orcid.org/0000-0003-4744-5421
MacRae, Calum A. - https://orcid.org/0000-0001-5181-2664
Mertins, Philipp - https://orcid.org/0000-0002-2245-528X
Obermayer, Benedikt - https://orcid.org/0000-0002-9116-630X
Rothe, Michael - https://orcid.org/0000-0002-6813-4705

References

1.	Burke MA, Cook SA, Seidman JG, Seidman CE. Clinical and Mechanistic Insights Into the Genetics of Cardiomyopathy. *Journal of the American College of Cardiology*. 2016;68:2871-2886. doi: 10.1016/j.jacc.2016.08.079

2.	Kuhnisch J, Herbst C, Al-Wakeel-Marquard N, Dartsch J, Holtgrewe M, Baban A, Mearini G, Hardt J, Kolokotronis K, Gerull B, et al. Targeted panel sequencing in pediatric primary cardiomyopathy supports a critical role of TNNI3. *Clinical genetics*. 2019;96:549-559. doi: 10.1111/cge.13645

3.	Ishibashi J, Seale P. Functions of Prdm16 in thermogenic fat cells. *Temperature*. 2015;2:65-72.

4.	Arndt AK, Schafer S, Drenckhahn JD, Sabeh MK, Plovie ER, Caliebe A, Klopocki E, Musso G, Werdich AA, Kalwa H, et al. Fine mapping of the 1p36 deletion syndrome identifies mutation of PRDM16 as a cause of cardiomyopathy. *American journal of human genetics*. 2013;93:67-77. doi: 10.1016/j.ajhg.2013.05.015

5.	Delplancq G, Tarris G, Vitobello A, Nambot S, Sorlin A, Philippe C, Carmignac V, Duffourd Y, Denis C, Eicher JC, et al. Cardiomyopathy due to PRDM16 mutation: First description of a fetal presentation, with possible modifier genes. *American journal of medical genetics Part C, Seminars in medical genetics*. 2020;184:129-135. doi: 10.1002/ajmg.c.31766

6.	van Waning JI, Caliskan K, Hoedemaekers YM, van Spaendonck-Zwarts KY, Baas AF, Boekholdt SM, van Melle JP, Teske AJ, Asselbergs FW, Backx A, et al. Genetics, Clinical Features, and Long-Term Outcome of Noncompaction Cardiomyopathy. *Journal of the American College of Cardiology*. 2018;71:711-722. doi: 10.1016/j.jacc.2017.12.019

7.	Long PA, Evans JM, Olson TM. Diagnostic Yield of Whole Exome Sequencing in Pediatric Dilated Cardiomyopathy. *J Cardiovasc Dev Dis*. 2017;4. doi: 10.3390/jcdd4030011

8.	Mazzarotto F, Hawley MH, Beltrami M, Beekman L, de Marvao A, McGurk KA, Statton B, Boschi B, Girolami F, Roberts AM, et al. Systematic large-scale assessment of the genetic architecture of left ventricular noncompaction reveals diverse etiologies. *Genet Med*. 2021;23:856-864. doi: 10.1038/s41436-020-01049-x

9.	Bjork BC, Turbe-Doan A, Prysak M, Herron BJ, Beier DR. Prdm16 is required for normal palatogenesis in mice. *Human molecular genetics*. 2010;19:774-789. doi: 10.1093/hmg/ddp543

10.	Wu T, Liang Z, Zhang Z, Liu C, Zhang L, Gu Y, Peterson KL, Evans SM, Fu XD, Chen J. PRDM16 Is a Compact Myocardium-Enriched Transcription Factor Required to Maintain Compact Myocardial Cardiomyocyte Identity in Left Ventricle. *Circulation*. 2022;145:586-602. doi: 10.1161/CIRCULATIONAHA.121.056666

11.	Jiang N, Yang M, Han Y, Zhao H, Sun L. PRDM16 Regulating Adipocyte Transformation and Thermogenesis: A Promising Therapeutic Target for Obesity and Diabetes. *Frontiers in pharmacology*. 2022;13:870250. doi: 10.3389/fphar.2022.870250

12.	Kajimura S, Seale P, Kubota K, Lunsford E, Frangioni JV, Gygi SP, Spiegelman BM. Initiation of myoblast to brown fat switch by a PRDM16-C/EBP-beta transcriptional complex. *Nature*. 2009;460:1154-1158. doi: 10.1038/nature08262

13.	Kajimura S, Seale P, Tomaru T, Erdjument-Bromage H, Cooper MP, Ruas JL, Chin S, Tempst P, Lazar MA, Spiegelman BM. Regulation of the brown and white fat gene programs through a PRDM16/CtBP transcriptional complex. *Genes & development*. 2008;22:1397-1409. doi: 10.1101/gad.1666108

14.	Seale P, Kajimura S, Spiegelman BM. Transcriptional control of brown adipocyte development and physiological function--of mice and men. *Genes & development*. 2009;23:788-797. doi: 10.1101/gad.1779209

15.	Seale P, Kajimura S, Yang W, Chin S, Rohas LM, Uldry M, Tavernier G, Langin D, Spiegelman BM. Transcriptional control of brown fat determination by PRDM16. *Cell metabolism*. 2007;6:38-54. doi: 10.1016/j.cmet.2007.06.001

16.	Harms MJ, Lim HW, Ho Y, Shapira SN, Ishibashi J, Rajakumari S, Steger DJ, Lazar MA, Won KJ, Seale P. PRDM16 binds MED1 and controls chromatin architecture to determine a brown fat transcriptional program. *Genes & development*. 2015;29:298-307. doi: 10.1101/gad.252734.114

17.	Seale P, Bjork B, Yang W, Kajimura S, Chin S, Kuang S, Scime A, Devarakonda S, Conroe HM, Erdjument-Bromage H, et al. PRDM16 controls a brown fat/skeletal muscle switch. *Nature*. 2008;454:961-967. doi: 10.1038/nature07182

18.	Heinig M, Adriaens ME, Schafer S, van Deutekom HWM, Lodder EM, Ware JS, Schneider V, Felkin LE, Creemers EE, Meder B, et al. Natural genetic variation of the cardiac transcriptome

713   in non-diseased donors and patients with dilated cardiomyopathy. *Genome biology.*
714   2017;18:170. doi: 10.1186/s13059-017-1286-z

715   19.   Pomaznoy M, Ha B, Peters B. GOnet: a tool for interactive Gene Ontology analysis. *BMC*
716   *Bioinformatics.* 2018;19:470. doi: 10.1186/s12859-018-2533-3

717   20.   Wang T, Xie X, Liu H, Chen F, Du J, Wang X, Jiang X, Yu F, Fan H. Pyridine nucleotide-
718   disulphide oxidoreductase domain 2 (PYROXD2): Role in mitochondrial function.
719   *Mitochondrion.* 2019;47:114-124. doi: 10.1016/j.mito.2019.05.007

720   21.   Khumukcham SS, Manavathi B. Two decades of a protooncogene HPIP/PBXIP1: Uncovering
721   the tale from germ cell to cancer. *Biochim Biophys Acta Rev Cancer.* 2021;1876:188576. doi:
722   10.1016/j.bbcan.2021.188576

723   22.   Tham YK, Bernardo BC, Huynh K, Ooi JYY, Gao XM, Kiriazis H, Giles C, Meikle PJ, McMullen
724   JR. Lipidomic Profiles of the Heart and Circulation in Response to Exercise versus Cardiac
725   Pathology: A Resource of Potential Biomarkers and Drug Targets. *Cell reports.* 2018;24:2757-
726   2772. doi: 10.1016/j.celrep.2018.08.017

727   23.   Wittenbecher C, Eichelmann F, Toledo E, Guasch-Ferre M, Ruiz-Canela M, Li J, Aros F, Lee
728   CH, Liang L, Salas-Salvado J, et al. Lipid Profiles and Heart Failure Risk: Results From Two
729   Prospective Studies. *Circulation research.* 2021;128:309-320. doi:
730   10.1161/CIRCRESAHA.120.317883

731   24.   Johnson TA, Jinnah HA, Kamatani N. Shortage of Cellular ATP as a Cause of Diseases and
732   Strategies to Enhance ATP. *Frontiers in pharmacology.* 2019;10:98. doi:
733   10.3389/fphar.2019.00098

734   25.   Xie N, Zhang L, Gao W, Huang C, Huber PE, Zhou X, Li C, Shen G, Zou B. NAD(+)
735   metabolism: pathophysiologic mechanisms and therapeutic potential. *Signal Transduct Target*
736   *Ther.* 2020;5:227. doi: 10.1038/s41392-020-00311-7

737   26.   Schunck WH, Konkel A, Fischer R, Weylandt KH. Therapeutic potential of omega-3 fatty acid-
738   derived epoxyeicosanoids in cardiovascular and inflammatory diseases. *Pharmacology &*
739   *therapeutics.* 2018;183:177-204. doi: 10.1016/j.pharmthera.2017.10.016

740   27.   Wang B, Wu L, Chen J, Dong L, Chen C, Wen Z, Hu J, Fleming I, Wang DW. Metabolism
741   pathways of arachidonic acids: mechanisms and potential therapeutic targets. *Signal*
742   *Transduct Target Ther.* 2021;6:94. doi: 10.1038/s41392-020-00443-w

743   28.   Cibi DM, Bi-Lin KW, Shekeran SG, Sandireddy R, Tee N, Singh A, Wu Y, Srinivasan DK,
744   Kovalik JP, Ghosh S, et al. Prdm16 Deficiency Leads to Age-Dependent Cardiac Hypertrophy,
745   Adverse Remodeling, Mitochondrial Dysfunction, and Heart Failure. *Cell reports.*
746   2020;33:108288. doi: 10.1016/j.celrep.2020.108288

747   29.   Nam JM, Lim JE, Ha TW, Oh B, Kang JO. Cardiac-specific inactivation of Prdm16 effects
748   cardiac conduction abnormalities and cardiomyopathy-associated phenotypes. *American*
749   *journal of physiology Heart and circulatory physiology.* 2020;318:H764-H777. doi:
750   10.1152/ajpheart.00647.2019

751   30.   Bruneau BG. Transcriptional regulation of vertebrate cardiac morphogenesis. *Circulation*
752   *research.* 2002;90:509-519. doi: 10.1161/01.res.0000013072.51957.b7

753   31.   Leszczynski P, Smiech M, Parvanov E, Watanabe C, Mizutani KI, Taniguchi H. Emerging
754   Roles of PRDM Factors in Stem Cells and Neuronal System: Cofactor Dependent Regulation
755   of PRDM3/16 and FOG1/2 (Novel PRDM Factors). *Cells.* 2020;9. doi: 10.3390/cells9122603

756   32.   Iida S, Chen W, Nakadai T, Ohkuma Y, Roeder RG. PRDM16 enhances nuclear receptor-
757   dependent transcription of the brown fat-specific Ucp1 gene through interactions with Mediator
758   subunit MED1. *Genes & development.* 2015;29:308-321. doi: 10.1101/gad.252809.114

759   33.   Seale P, Conroe HM, Estall J, Kajimura S, Frontini A, Ishibashi J, Cohen P, Cinti S,
760   Spiegelman BM. Prdm16 determines the thermogenic program of subcutaneous white
761   adipose tissue in mice. *The Journal of clinical investigation.* 2011;121:96-105. doi:
762   10.1172/JCI44271

763   34.   Mugoni V, Postel R, Catanzaro V, De Luca E, Turco E, Digilio G, Silengo L, Murphy MP,
764   Medana C, Stainier DY, et al. Ubiad1 is an antioxidant enzyme that regulates eNOS activity by
765   CoQ10 synthesis. *Cell.* 2013;152:504-518. doi: 10.1016/j.cell.2013.01.013

766   35.   Nam D, Chatterjee S, Yin H, Liu R, Lee J, Yechoor VK, Ma K. Novel Function of Rev-erbalpha
767   in Promoting Brown Adipogenesis. *Scientific reports.* 2015;5:11239. doi: 10.1038/srep11239

768   36.   Zhao Y, Lu X, Wan F, Gao L, Lin N, He J, Wei L, Dong J, Qin Z, Zhong F, et al. Disruption of
769   Circadian Rhythms by Shift Work Exacerbates Reperfusion Injury in Myocardial Infarction.
770   *Journal of the American College of Cardiology.* 2022;79:2097-2115. doi:
771   10.1016/j.jacc.2022.03.370

772   37.   Lou B, Boger M, Bennewitz K, Sticht C, Kopf S, Morgenstern J, Fleming T, Hell R, Yuan Z,
773   Nawroth PP, et al. Elevated 4-hydroxynonenal induces hyperglycaemia via Aldh3a1 loss in

zebrafish and associates with diabetes progression in humans. *Redox biology*. 2020;37:101723. doi: 10.1016/j.redox.2020.101723

38. Abramovich C, Shen WF, Pineault N, Imren S, Montpetit B, Largman C, Humphries RK. Functional cloning and characterization of a novel nonhomeodomain protein that inhibits the binding of PBX1-HOX complexes to DNA. *The Journal of biological chemistry*. 2000;275:26172-26177. doi: 10.1074/jbc.M001323200

39. Wang X, Yang Z, Zhang H, Ding L, Li X, Zhu C, Zheng Y, Ye Q. The estrogen receptor-interacting protein HPIP increases estrogen-responsive gene expression through activation of MAPK and AKT. *Biochimica et biophysica acta*. 2008;1783:1220-1228. doi: 10.1016/j.bbamcr.2008.01.026

40. Moreno D, Viana R, Sanz P. Two-hybrid analysis identifies PSMD11, a non-ATPase subunit of the proteasome, as a novel interaction partner of AMP-activated protein kinase. *The international journal of biochemistry & cell biology*. 2009;41:2431-2439. doi: 10.1016/j.biocel.2009.07.002

41. Grimes KA, Pyo A, Molkentin JD. Abstract 918: Pre-B-cell Leukemia Homeobox Interacting Protein 1 is a Novel Regulator of Growth Signaling in the Heart. *Circulation research*. 2019;125.

42. Alankarage D, Szot JO, Pachter N, Slavotinek A, Selleri L, Shieh JT, Winlaw D, Giannoulatou E, Chapman G, Dunwoodie SL. Functional characterization of a novel PBX1 de novo missense variant identified in a patient with syndromic congenital heart disease. *Human molecular genetics*. 2020;29:1068-1082. doi: 10.1093/hmg/ddz231

43. Van Bergen NJ, Hock DH, Spencer L, Massey S, Stait T, Stark Z, Lunke S, Roesley A, Peters H, Lee JY, et al. Biallelic Variants in PYROXD2 Cause a Severe Infantile Metabolic Disorder Affecting Mitochondrial Function. *International journal of molecular sciences*. 2022;23. doi: 10.3390/ijms23020986

44. O'Grady GL, Best HA, Sztal TE, Schartner V, Sanjuan-Vazquez M, Donkervoort S, Abath Neto O, Sutton RB, Ilkovski B, Romero NB, et al. Variants in the Oxidoreductase PYROXD1 Cause Early-Onset Myopathy with Internalized Nuclei and Myofibrillar Disorganization. *American journal of human genetics*. 2016;99:1086-1105. doi: 10.1016/j.ajhg.2016.09.005

45. Caspi T, Straw S, Cheng C, Garnham JO, Scragg JL, Smith J, Koshy AO, Levelt E, Sukumar P, Gierula J, et al. Unique Transcriptome Signature Distinguishes Patients With Heart Failure With Myopathy. *Journal of the American Heart Association*. 2020;9:e017091. doi: 10.1161/JAHA.120.017091

46. Berndt N, Eckstein J, Wallach I, Nordmeyer S, Kelm M, Kirchner M, Goubergrits L, Schafstedde M, Hennemuth A, Kraus M, et al. CARDIOKIN1: Computational Assessment of Myocardial Metabolic Capability in Healthy Controls and Patients With Valve Diseases. *Circulation*. 2021;144:1926-1939. doi: 10.1161/CIRCULATIONAHA.121.055646

47. Walker CJ, Schroeder ME, Aguado BA, Anseth KS, Leinwand LA. Matters of the heart: Cellular sex differences. *Journal of molecular and cellular cardiology*. 2021;160:42-55. doi: 10.1016/j.yjmcc.2021.04.010

48. Lopaschuk GD, Karwi QG, Tian R, Wende AR, Abel ED. Cardiac Energy Metabolism in Heart Failure. *Circulation research*. 2021;128:1487-1513. doi: 10.1161/CIRCRESAHA.121.318241

49. Sosnowski DK, Jamieson KL, Darwesh AM, Zhang H, Keshavarz-Bahaghighat H, Valencia R, Viveiros A, Edin ML, Zeldin DC, Oudit GY, et al. Changes in the Left Ventricular Eicosanoid Profile in Human Dilated Cardiomyopathy. *Front Cardiovasc Med*. 2022;9:879209. doi: 10.3389/fcvm.2022.879209
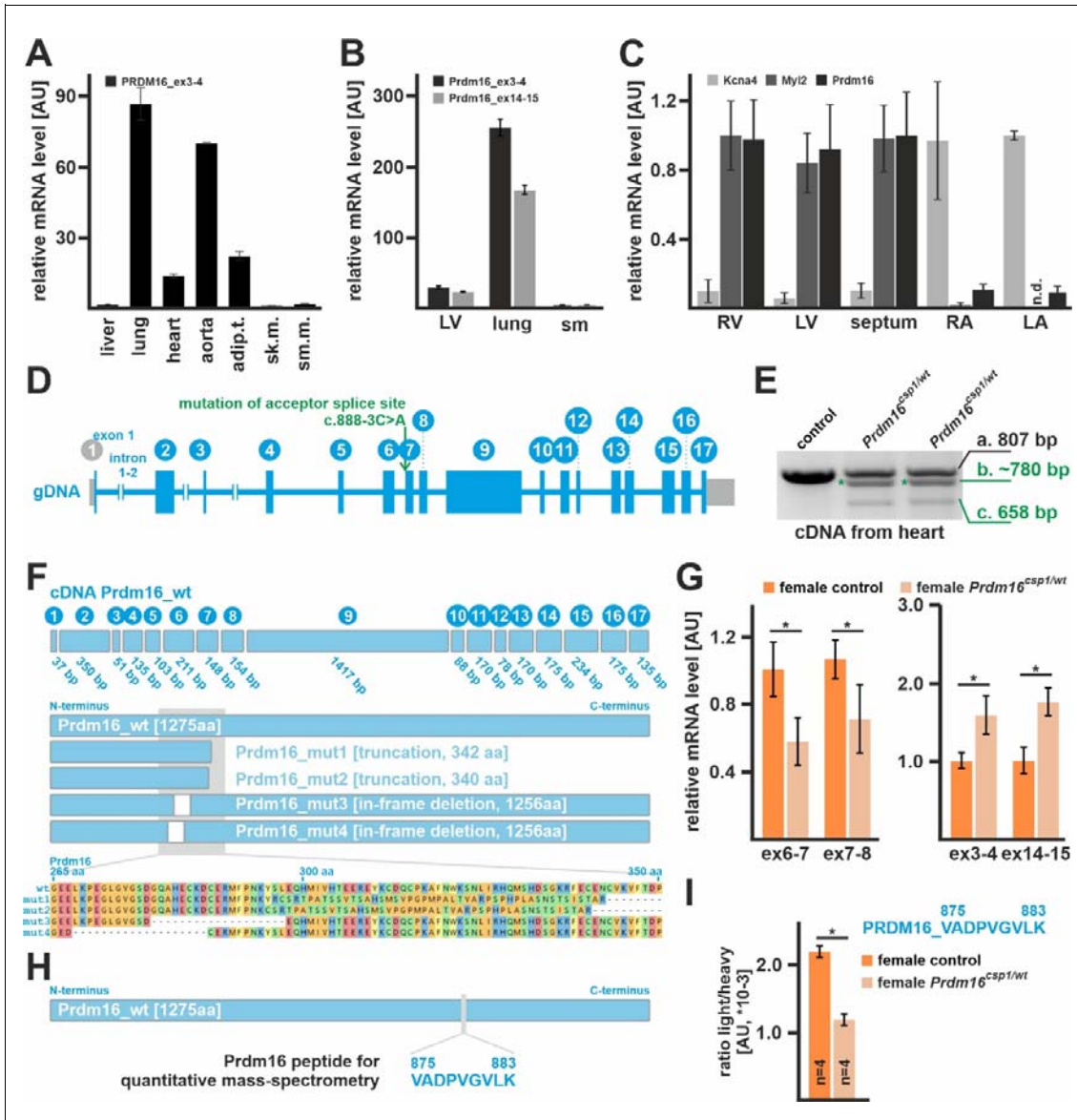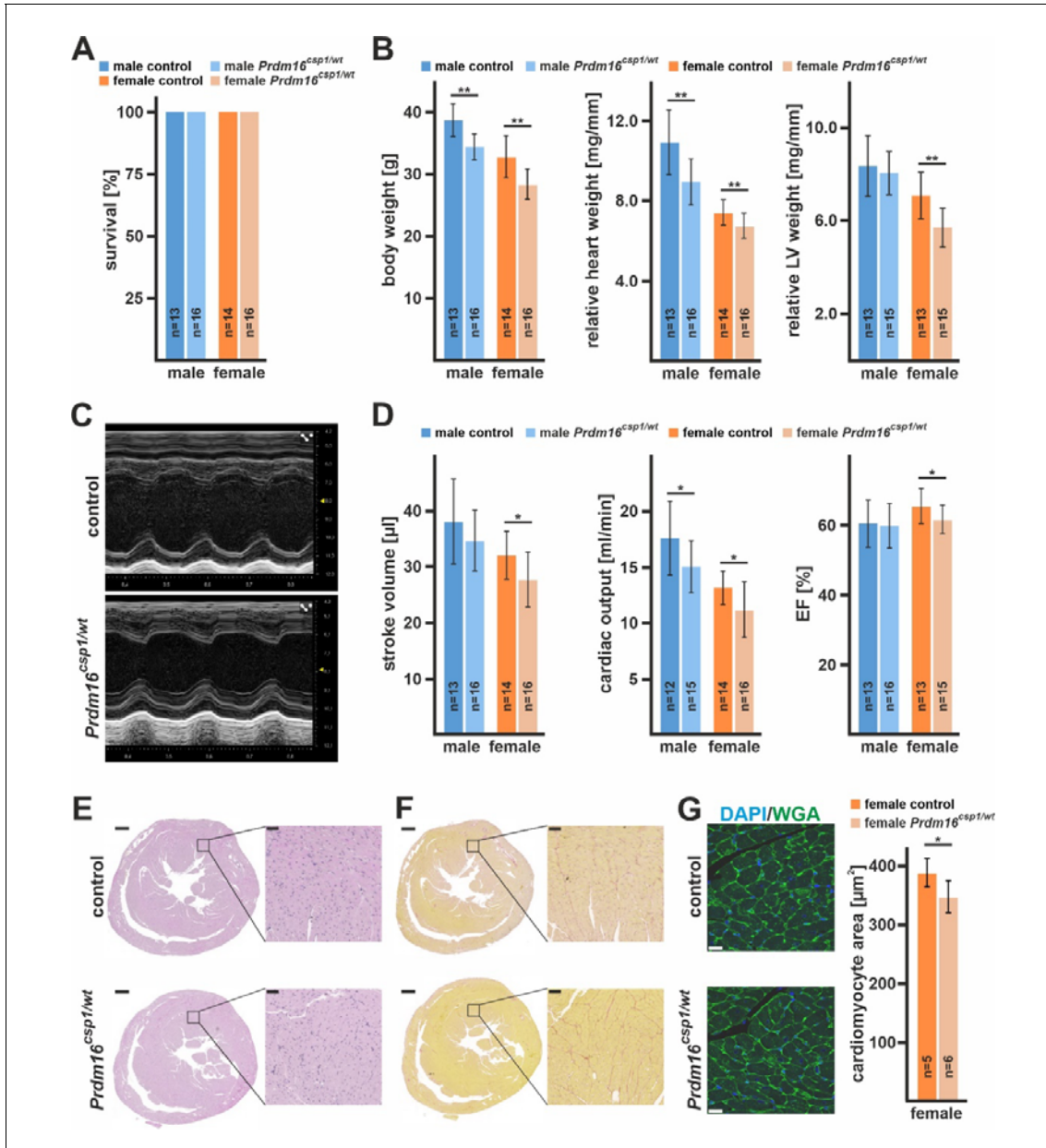
822 **Figures**

Figure 1. Expression of *Prdm16* in the heart of *Prdm16^csp1/wt* mice. (A) Expression analysis reveals high *PRDM16* transcript levels in human lung, aorta, adipose tissue (adip.t.), and heart. Liver, skeletal muscle (sk.m.), and smooth muscle (sm.m.) show low *PRDM16* expression. **(B)** *Prdm16* is highly expressed in murine lung tissue, shows robust levels in the left ventricle (LV) but low expression in skeletal muscle (sm). **(C)** *Prdm16* is robustly expressed in LV, right ventricle (RV), and the septum. The left (LA) and right atrium (RA) does not show considerable *Prdm16* expression. *Kcna4* and *Myl2* transcripts demonstrate atrial and ventricular tissue origin. **(D)** The murine *Prdm16* gene comprises 17 exons and *Prdm16^csp1/wt* mice carry the point mutation c.888-3C>A affecting the acceptor splice site of intron_6-7. **(E)** PCR genotyping with heart cDNA from heterozygous *Prdm16^csp1/wt* mice generates 3 products: a) wild-type fragment (807 bp), b) unknown mutant product (~780 bp, *), and c) mutant product without exon 7 (658 bp). **(F)** The wild-type Prdm16 protein is 1275 amino acids (aa) long. Targeted high-throughput sequencing of the different PCR products identifies four main Prdm16 mutant proteins in *Prdm16^csp1/wt* mice including truncation (mut1, mut2) and in-frame deletion (mut3, mut4) variants (Figure I and II in the Data Supplement, for detailed Results see Data Supplement). **(G)** Quantitative detection of *Prdm16* transcript levels with qPCR detectors targeting the exon

7 deletion region shows approx. 40-50% reduced expression. In contrast, PCR detectors targeting exon3-4 and exon14-15 identifies increased *Prdm16* levels. Analysis was performed on female *Prdm16*$^{csp1/wt}$ heart tissue. **(H)** Detection of Prdm16 protein was achieved by PRM (parallel-reaction monitoring) using the Prdm16 derived peptide V875-K883. **(I)** Quantitation of Prdm16 peptide in control and *Prdm16*$^{csp1/wt}$ lung tissue. The ratio of endogenous (light) and standard spike-in (heavy) peptide is shown. Statistical analysis was performed with unpaired t-test (p<0.05).
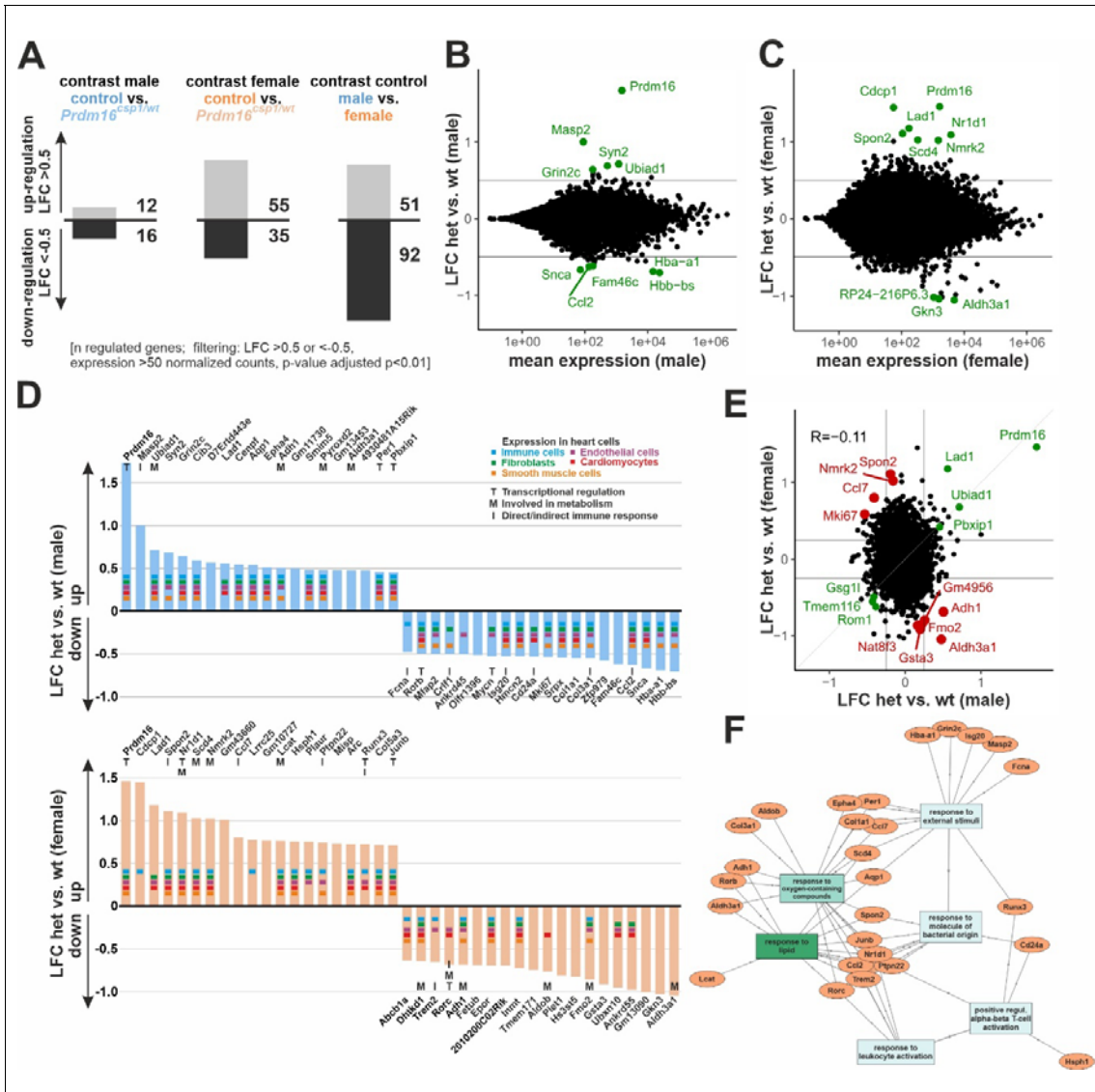
823

824

Figure 2. Diminished cardiac performance after *Prdm16* inactivation. (A) Survival of male and female *Prdm16^csp1/wt^* mice is normal until the age of 8 month. **(B)** 8-month-old *Prdm16^csp1/wt^* mice of both sexes have a reduced absolute body weight. Normalization against tibia length demonstrated a diminished relative heart and LV weight in *Prdm16^csp1/wt^* mutants. **(C)** M-mode images illustrate the heart phenotype in *Prdm16^csp1/wt^* mice as assessed with echocardiography. **(D)** At the age of 8 months *Prdm16^csp1/wt^* mice of both sexes have diminished cardiac function as illustrated by stroke volume, cardiac output, and ejection fraction (EF). Full echocardiography data are available Tables IV-VI in the Data Supplement. **(E)** Histological analysis with H&E staining reveals normal tissue organization in female *Prdm16^csp1/wt^* hearts. Scale bars in E and F are 500 μm (full heart) and 50 μm (inset). **(F)** Histological staining for fibrosis with Picro-Sirius red is negative in female *Prdm16^csp1/wt^* heart tissue. **(G)** The cell area of female heart muscle (cross sections) stained with wheat-germ agglutinin (WGA, green) is significantly reduced. Nuclei were stained with DAPI (blue). Scale bar is 20 μm. Statistical analysis was performed with unpaired t-test (p<0.05).

Figure 3. Transcriptome analysis of *Prdm16csp1/wt* heart tissue. (A) Transcriptome analysis with RNAseq of *Prdm16csp1/wt* LV shows in male 28 and in female 90 differentially regulated genes compared to controls. Analysis of male vs. female control hearts identifies 143 differentially regulated transcripts. **(B-C)** Bioinformatic filtering ranked the normalized log2 cpk according the absolute log2 fold change (LFC) after elimination of regulated targets with an adjusted p-value (padj) $<10^{-2}$. Scatterplots show the LFC against mean expression for the contrast *Prdm16csp1/wt* (het) vs controls (wt) in male (B) or female (C) heart. The top 10 differentially regulated genes (adj. p < 0.01) are highlighted in green and labeled. **(D)** Summary of top 20 up- and down-regulated genes in male (upper panel) and female (lower panel) hearts. Expression of selected genes in cardiac cell types is annotated according to the color code. Functional association with transcription (T), metabolism (M), and immune response (I) is shown for relevant genes. **(E)** Scatterplot shows the LFC detected in A and B against each other. Genes with concordant changes (abs LFC > 0.25) are highlighted in green, genes with discordant changes (top 10; adj. p < 0.01) are highlighted in red. The overall correlation is R=-0.11 (n=21276). **(F)** Gene ontology (GO) network was constructed with GOnet[19] by using the male and female TOP20 up- and down-regulated genes in *Prdm16csp1/wt* hearts. GO terms *response to lipids* and *response to oxygen-containing compounds* show strongest association.
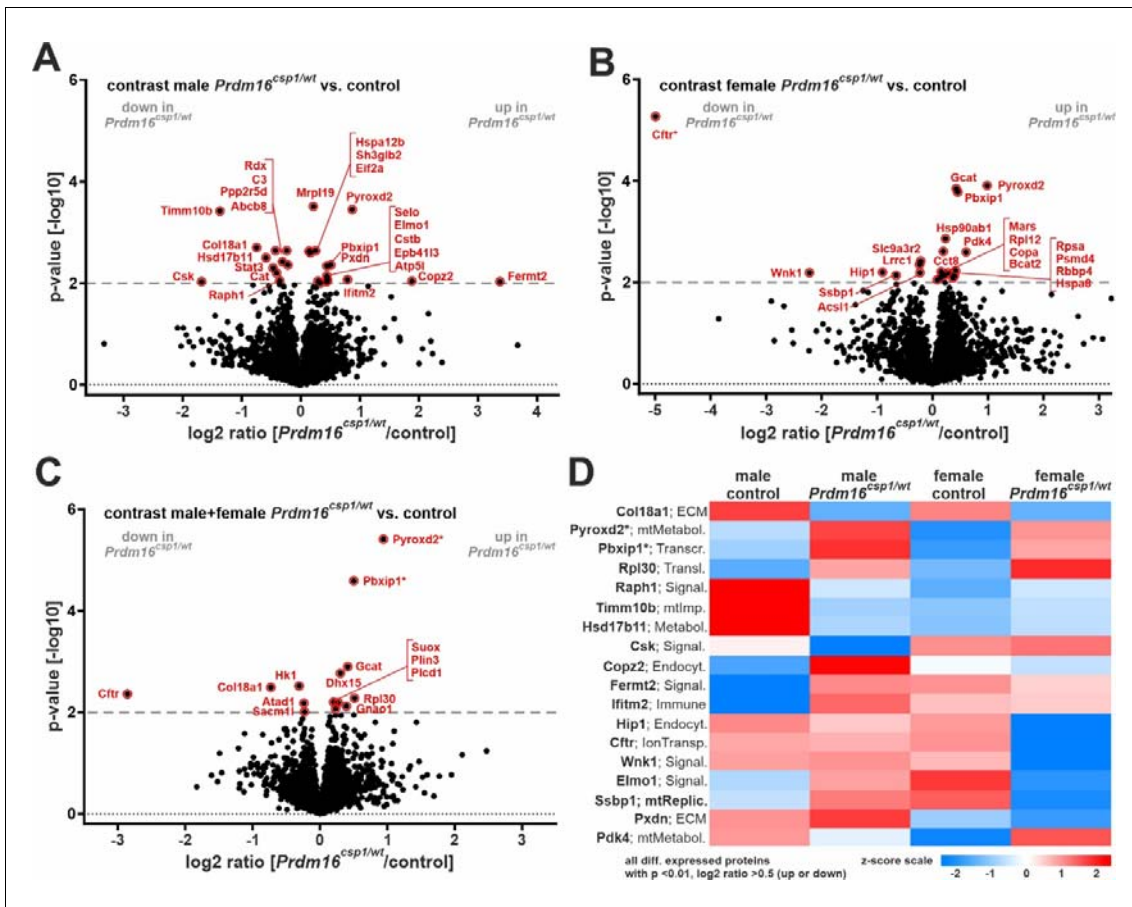
825

Figure 4. Proteome comparison of *Prdm16$^{csp1/wt}$* cardiac tissue. Volcano plots for *Prdm16$^{csp1/wt}$*/control pairwise comparisons with log2 ratio (x-axis) and p-value (y-axis) of male hearts **(A)**, female hearts **(B)**, and combined analysis of male+female hearts **(C)**. Red coloring indicates significantly altered proteins (threshold dashed grey line, p-value <0.01) and * highlights highly significantly different proteins with p-value <0.0001. **(D)** Heat map of all regulated proteins (p-value <0.01, abs log2 ratio >0.5) using z-scored values of group median intensity. Pre B-cell leukemia transcription factor interacting protein 1 (Pbxip1) and pyridine nucleotide-disulphide oxidoreductase domain 2 (Pyroxd2) are consistently increased in male and female *Prdm16$^{csp1/wt}$* mice with p-value <0.0001.
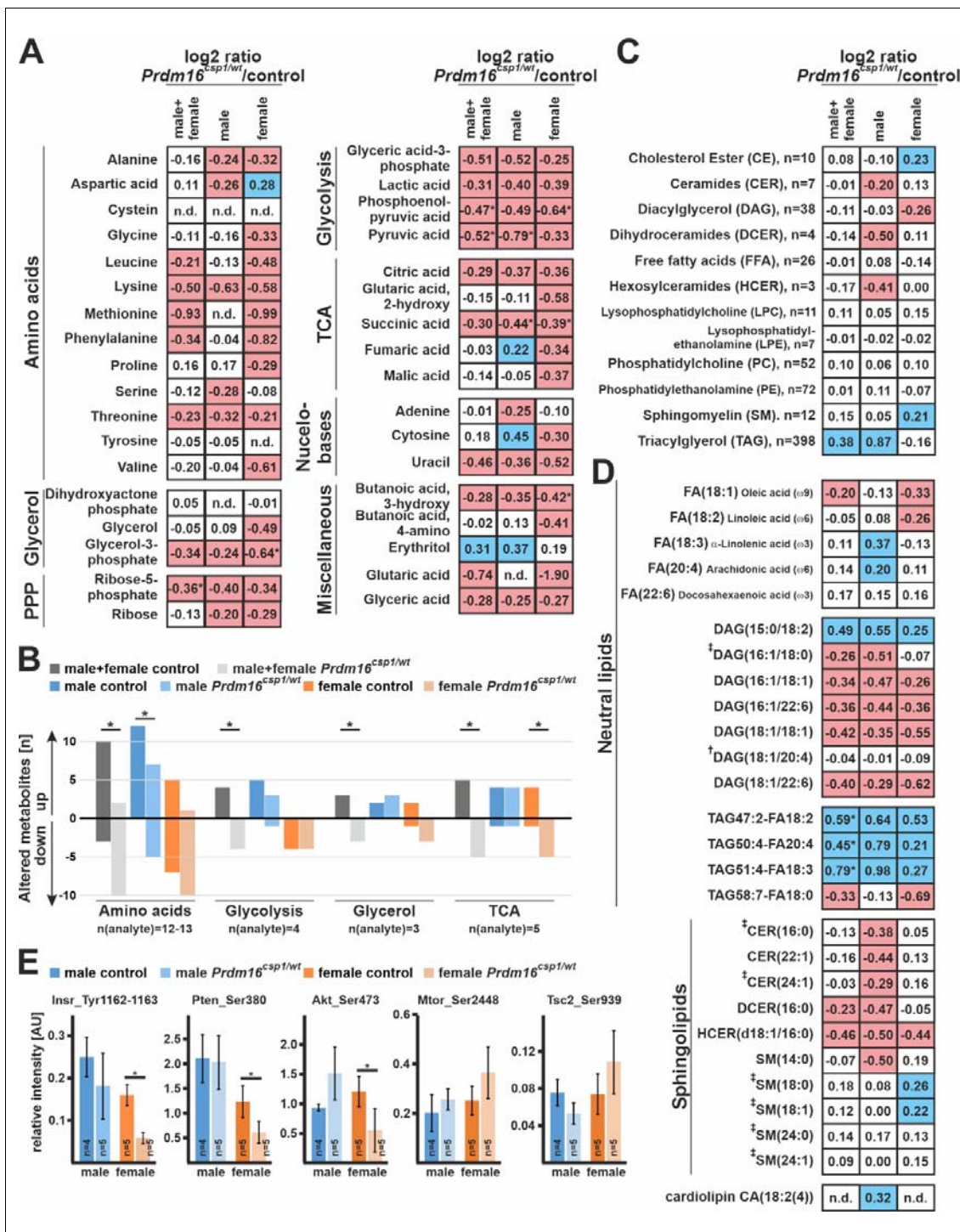
826

Figure 5. Altered metabolism in *Prdm16csp1/wt* cardiac tissue. (A) Normalized central carbon metabolite counts are presented as log2 value of the mean of normalized peak area ratio *Prdm16csp1/wt*/controls of males, females, and combination of both sexes. In female *Prdm16csp1/wt* LV tissue, broad suppression of several metabolic pathways was observed. In male *Prdm16csp1/wt* LV tissue, a similar but less pronounced reduction was detected. Statistical analysis of individual metabolites was performed with non-parametric Wilcoxon Rank Sum test, *indicates p<0.05. **(B)** Univariate analysis reveals in cardiac tissue of *Prdm16csp1/wt* mice significant reduction of the amino acid, glycolysis, glycerol, and tricarboxylic acid cycle (TCA) metabolism using combined male and female data. Divergent metabolism of male and female animals was observed for amino acid

metabolism, glycolysis, and TCA cycle. **(C)** Lipid analysis was performed with LC-MS using the lipidizer kit (Sciex). Global lipid analysis and evaluation as log2 value of the intensity ratio *Prdm16$^{csp1/wt}$*/controls reveals normal levels for most lipid classes. Strongest regulation was observed for triacylglycerol (TAG) in male *Prdm16$^{csp1/wt}$* hearts. The number (n) of validly detected lipids per class is indicated. **(D)** Selected neutral lipids and sphingolipids critical for the heart, lipids altered in *Prdm16$^{csp1/wt}$* mice, and lipids previously associated with heart function ([†]*Tham* et al. [22], [‡]*Wittenbecher* et al. [23]) are presented for *Prdm16$^{csp1/wt}$* cardiac tissue of both sexes and in combination. Values for phospholipids are available in Figure IX in the Data Supplement. **(E)** Signaling activity of the mitogen-activated protein kinase (MAPK) and mTOR pathway was assessed with the Milliplex phosphoprotein magnetic bead system and revealed diminished phosphorylation of insulin receptor (Insr_Tyr1162-1163), phosphatase and tensin homolog (Pten_Ser380), and Akt serine/threonine kinase 2 (Akt_Ser473) in female *Prdm16$^{csp1/wt}$* mice. Statistical analysis of selected lipids was performed with non-parametric Wilcoxon Sum Rank test, * indicates $p<0.05$. Coloring indicates reduction (red) or increase (blue) of the log2 of ratio by -0.2 or 0.2, respectively.
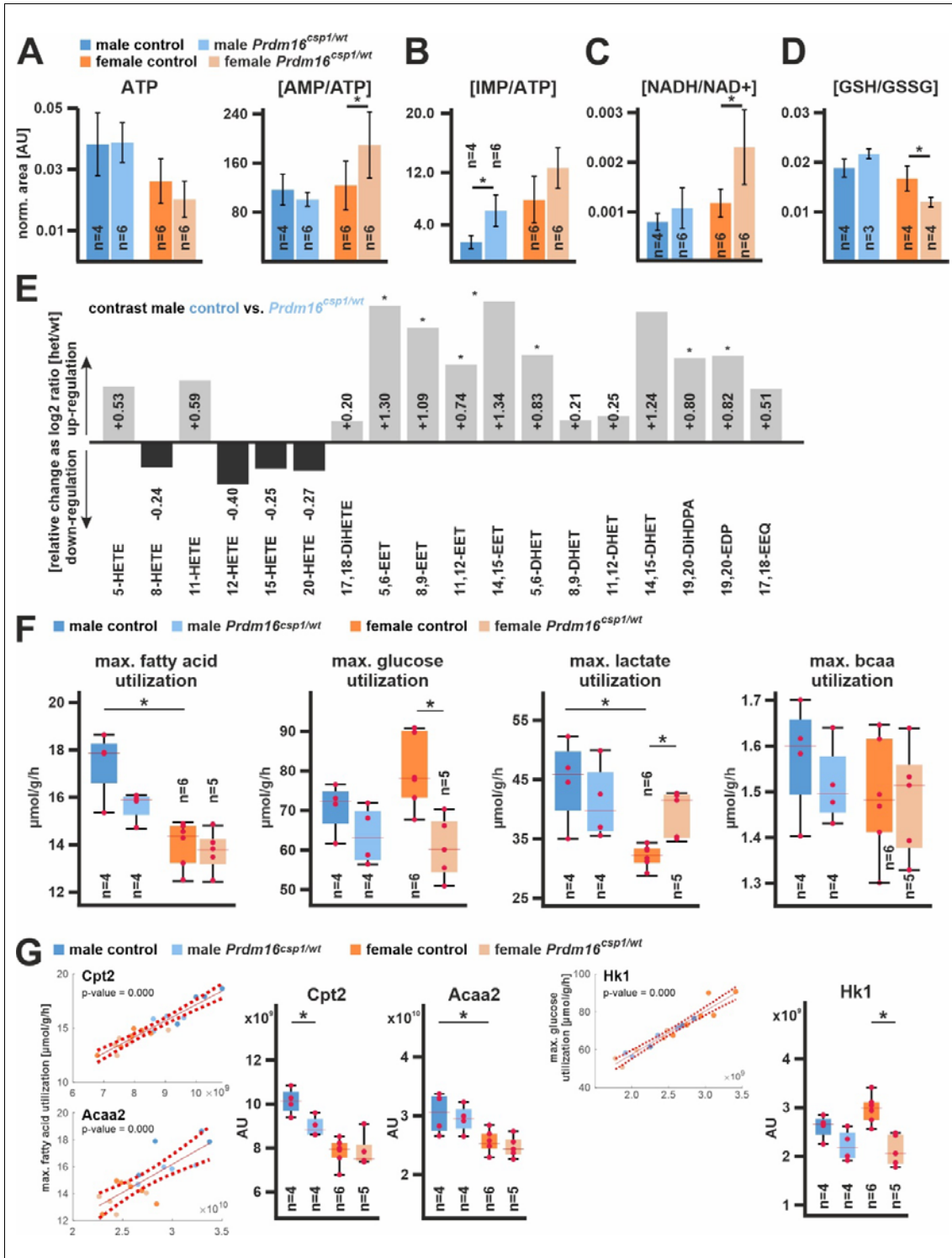
827

828

829

Figure 6. Nutrient metabolism in *Prdm16csp1/wt* cardiac tissue. (A) Assessment of metabolites critical for energy metabolism using LV tissue and LC-MS. Normalized values are shown for adenosine triphosphate (ATP) and the ratio of adenosine monophosphate (AMP) vs. ATP (AMP/ATP). **(B)** The ratio of inosine monophosphate (IMP) vs. ATP (IMP/ATP) is increased in *Prdm16csp1/wt* hearts. **(C)** The ratio of reduced vs. oxidized nicotinamide adenine dinucleotide (NADH/NAD+) is increased in female *Prdm16csp1/wt* hearts. **(D)** Oxidative capacity of cardiac tissues was assessed with the ratio of reduced vs.

oxidized glutathione (GSH/GSSG). Female *Prdm16$^{csp1/wt}$* hearts show a significantly reduced GSH/GSSG ratio. **(E)** Eicosanoids were measured in male *Prdm16$^{csp1/wt}$* hearts with LC/ESI-MS-MS. Data are presented as log2 *Prdm16$^{csp1/wt}$*/controls ratio with down- or up-regulation as black or grey bars, respectively. All epoxyeicosatrienoic (EET) and dihydroxyeicosatrienoic (DHET) acids are increased in *Prdm16$^{csp1/wt}$* cardiac tissue. Corresponding absolute measurements are available in Table VIII in the Data Supplement. **(F)** Modelling of major cardiac metabolic processes occurred with CARDIOKIN1 [46] using protein expression data. Differences in maximal substrate utilization for fatty acids (FA), glucose, lactate, and branched chain amino acids (bcaa). Box plots show median and 25% quartile. Red dots depict maximal capacities for individual animals. **(G)** Individual protein impact for FA and glucose metabolism was correlated for carnitine palmitoyltransferase 2 (Cpt2), acetyl-CoA acyltransferase 2 (Acaa2), and hexokinase 1 (Hk1) using linear regression analysis of the maximal substrate utilization vs. protein abundance (red dashed line indicates confidence interval, 95%). Box plots show median and 25% quartile. Red dots depict Cpt2, Acaa2, and Hk1 maximal capacities for individual animals. Statistical analysis of individual metabolites and processes was performed with unpaired t-test, * indicates $p < 0.05$.

830

831

832

	Control *Prdm16*	Monoallelic *Prdm16* deficiency	Biallelic *Prdm16* deficiency
Mouse models		$Prdm16^{csp1/wt}$	$Prdm16^{csp1/csp1}$ $Xmlc2Cre;Prdm16^{flox/flox}$ $Mesp1Cre;Prdm16^{flox/flox}$
Survival	unaffected	unaffected	postnatal or premature death
Cardiac function	unaffected	↓	↓↓
Heart size	unaffected	hypoplasia	hypoplasia (early stage) hypertrophy (late stage)
Metabolism	unaffected	males fatty acid females glucose ↓	glucose & fatty acid metabolism ↓↓
Mitochondria	unaffected	unaffected	mitochondrial dysfunction
Oxidative stress	unaffected	↑	↑
Molecular mechanism		upregulation Pyroxd2, Pbxip	upregulation hypertrophy genes Nppa/Nppb, Myh7 upregulation trabeculation genes
Sex		females more affected compared to males (early stage pathology)	not investigated

Figure 7. Prdm16 is an early regulator of cardiac metabolism. Assessing different mouse models for the *PRDM16* associated cardiomyopathy reveals distinct cardiac phenotypes after mono- or biallelic Prdm16 inactivation. Metabolism is differentially affected at early (*Prdm16^{csp1/wt}*) and late pathology stage (*Xmlc2Cre;Prdm16^{flox/flox}*, *Mesp1Cre;Prdm16^{flox/flox}*).[10,28]

833